Unlocking the origin of stability and superconductivity in $LaBeH_8$ at submegabar pressure

Zefang Wang,[1] Hong jian Zhao,[1] Xin Zhong,[1,*] Hanyu Liu,[1,2,3,†] and Yanming Ma[1,2,3,‡]

[1]*Key Laboratory of Material Simulation Methods and Software of Ministry of Education, College of Physics, Jilin University, Changchun 130012, China*

[2]*State Key Laboratory of Superhard Materials, College of Physics, Jilin University, Changchun 130012, China*

[3]*International Center of Future Science, Jilin University, Changchun 130012, China*

(Received 1 April 2024; revised 19 May 2024; accepted 24 May 2024; published 10 June 2024)

The recent synthesis of $LaBeH_8$ with a superconducting critical temperature (T_c) up to 110 K at a pressure of 80 GPa generates great hope to achieve high-temperature superconductivity in ternary hydrides at submegabar pressure. However, the underlying mechanism governing its unexpected stability and high-temperature superconductivity remains elusive, which impedes the demanding design of other high-T_c ternary hydrides on the way to room-temperature superconductivity. Here, we conducted a comprehensively theoretical study to reveal the origin of the stability and superconductivity of $LaBeH_8$. We found that $LaBeH_8$ could be viewed as a rocksalt compound of $La^{2+}[BeH_8]^{2-}$ and its unexpected stability lies in the emergence of an unusually negatively charged molecular $[BeH_8]^{2-}$ unit containing polarized Be-H covalent bonds. This $[BeH_8]^{2-}$unit gives rise to an intrinsic metallic feature in the solid, and its interaction with neighboring ones via weak H-H coupling contributes mostly to the high-temperature superconductivity. Our current results offer a key perspective of high-temperature superconductivity among ternary hydrides, thus inspiring a potential developing strategy to design high-T_c hydrides via the exploration of similar intrinsic metallic salt structure motifs containing a variety of hydrogen-rich covalent units.

DOI: 10.1103/PhysRevB.109.214506

I. INTRODUCTION

The quest for high-temperature superconductors has attracted great attention in the field of physics, chemistry, and materials science. Of particular interest in recent decades is to focus on the prediction and synthesis of hydrogen-based superconductors at megabar pressures [1–11]. It is noteworthy that a computational study via structure-searching simulations [12,13] established a compelling hydride CaH_6, which was characterized by an unusual H_{24} caged framework and regarded as the first example of a high critical temperature (T_c) clathrate hydride superconductor [14]. This groundbreaking compound was confirmed with T_c values reaching up to 215 K at 170 GPa by two very recent experimental works [15,16]. This computational prediction provides guidance in the search for a high-temperature superconductor among hydrogen-rich compounds with a quintessential hydrogen-cage framework. On this basis, a great many clathrate metal hydrides have been predicted, and then successfully synthesized in the following experiments, such as YH_6 [17–21], YH_9 [17,19,21,22], and LaH_{10} [17,23–25] with T_c above 200 K.

Over a decade ago, several studies endeavored to realize high-temperature superconductivity in ternary hydrides, while the predicted or measured T_c is not high, such as $BaReH_9$ [26–28] and Li_5MoH_{11} [29] with T_c below 7 K. Until recently, motivated by structure-searching simulations [30–40], there has been a breakthrough with the successful synthesis of $Fm\bar{3}m$-$LaBeH_8$ boasting the highest T_c of 110 K at a pressure of 80 GPa [41], and setting a record-high superconductivity among ternary hydrides at submegabar pressures. However, despite this significant advancement, the mechanism governing the superconductivity and unexpected stability of $LaBeH_8$ remains elusive. Further comprehensive studies are imperative to unravel these complexities, as they hold the key to advancing the future design of high-T_c hydrides at near-ambient or even ambient pressures.

In this paper, our comprehensive study reveals that the stability of $LaBeH_8$ can be regarded as a $[BeH_8]^{2-}$ salt-like configuration. Electronic simulations indicate that these $[BeH_8]^{2-}$ units exhibit an intrinsic metallic feature and the hydrogen in $[BeH_8]^{2-}$ mimics the electronic behavior of metallic atomic hydrogen [42–46], which results in a high hydrogen-dominated density of states at the Fermi level (E_f). Further analysis indicates that there is strong coupling between the H-derived electronic states at E_f and the phonons originating from inter-BeH_8 H-H vibrations between these peculiar $[BeH_8]^{2-}$ units. This strong electron-phonon coupling (EPC) plays a critical role in high-temperature superconductivity. To this end, we discuss the origin of stability observed in $LaBeH_8$, attributing it to the emergence of covalent $[BeH_8]^{2-}$ units at submegabar pressures. These results provide guidance for the further exploration of high-temperature superconductivity among intrinsic metallic ternary hydrides with similar salt structure motifs.

*zhongxin@calypso.cn
†hanyuliu@jlu.edu.cn
‡mym@jlu.edu.cn

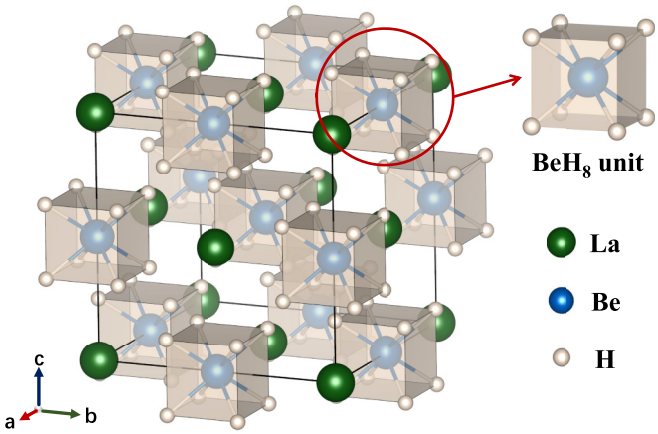

FIG. 1. Stoichiometric $LaBeH_8$ ternary hydride consists of La atoms and BeH_8 units.

II. COMPUTATIONAL DETAILS

Structural optimization and computations of electronic properties were all performed in the framework of density functional theory (DFT) as implemented in the VASP code [47]. The Perdew-Burke-Ernzerhof functional [48] within the generalized gradient approximation (GGA) [49] was employed and a kinetic cutoff energy of 600 eV was adopted. A Monkhorst-Pack k-point mesh with a density of $2\pi \times 0.02$ Å^{-1} was used for all structures in this work. For example, this density corresponds to a k-point mesh of $16 \times 16 \times 16$ for a primitive cell of $LaBeH_8$ at 80 GPa. Bonding in $LaBeH_8$ was investigated by the crystal orbital Hamiltonian population (COHP) analysis using the LOBSTER code [50], which provides an atom-specific measure of the bonding character of states in a given energy region. The molecular orbital (MO) and visualized wave functions were computed taking advantage of the VASPKIT code [51]. Vibrational and superconducting properties were calculated using density functional perturbation theory (DFPT) [52], as implemented in the QUANTUM ESPRESSO (QE) package [53]. Ultrasoft pseudopotentials [54] were used with a kinetic energy cutoff of 80 Ry and a charge density cutoff of 960 Ry. The charge density was integrated on a Γ-centered $24 \times 24 \times 24$ k-point mesh. Moreover, we have also performed additional simulations to ensure the consistency of simulations by using VASP and QE. We found the energy difference between VASP and QE is less than 0.5 meV, which indicates the validation of our computational scheme. Electron-phonon coupling (EPC) and vibrational properties were calculated by employing a $6 \times 6 \times 6$ Γ-centered q-point mesh. A Methfessel-Paxton first-order smearing of 0.02 Ry was applied. The superconducting gap and T_c value were calculated from the Allen-Dynes modified McMillan [55] equation and Eliashberg equations [56].

III. RESULTS AND DISCUSSION

In view of the crystal structure on $LaBeH_8$, this compound is found to adopt the rocksalt structure with a symmetry space group of $Fm\bar{3}m$, where La atoms and BeH_8 cubic units occupy the sites identical to those of Na^+ and Cl^- ions in the well-known table salt, as shown in Fig. 1. We found that distances between hydrogen atoms (1.54 and 1.64 Å) in $LaBeH_8$ at 80 GPa are much larger than those of typical H-H distances (1.1–1.3 Å) that characterizes a clathrate structure observed in hydrogen-rich superconductors [11]. In order to gain a deeper understanding of the chemical bonding on $LaBeH_8$, we have carried out two types of bonding analysis calculations of the electron localization function (ELF) [57] and integrated crystalline orbital Hamiltonian population (ICOHP) [58] at 80 GPa, which are often regarded as insightful tools for the analysis of chemical bonding. As shown in Fig. S1 and Table S1 [59], in $LaBeH_8$, there is no localized electron existing between the two nearest H atoms where the ELF value is small at 0.33 and the −ICOHP values between two nearest H atoms are negligibly small at 0.2. For a good comparison, in the known clathrate structure of LaH_{10}, the electron localization with an ELF value larger than 0.66 [60] and the large −ICOHP value at 1.6 are evident, leading to a good characterization of a clathrate structure. Based on all these results, the likelihood of $LaBeH_8$ being a clathrate structure as claimed in previous studies is safely excluded.

As demonstrated in the ELF simulations (Fig. S1) [59], the results also show the strong polarized covalent bonding between Be and H atoms, which indicates the BeH_8 cube is a covalent molecular unit and thus supports the subsequent analysis on the electronic property of the molecular BeH_8 unit. Moreover, the quite low ELF value between La and H atoms, together with the large La-H distance of 2.23 Å, highlights the ionic bonding feature between La and H atoms. These findings suggest that this structure could be regarded as a saltlike structure of $La^{x+}[BeH_8]^{x-}$, which motivates us to estimate the valence states of $[BeH_8]^{x-}$ and La^{x+}, despite $LaBeH_8$ being a metallic compound. We thus performed electronic simulations on the projected electronic density of states (DOS) and its integral value below the Fermi level (E_f), as shown in Fig. 2(a) and Table S2 [59]. The results reveal that there are almost entire electrons ($2e^-$) from the 6s orbital of the La atom being transferred to the BeH_8 unit, where the La atom has three valence electrons with an electronic configuration of $5d^16s^2$. As a consequence, all the results suggest that $LaBeH_8$ could be viewed as a saltlike configuration of $La^{2+}[BeH_8]^{2-}$.

It is noted that there is a high hydrogen-dominated density of states (DOS) at the Fermi level (E_f) in $LaBeH_8$ as shown in Fig. 2(a), which is often strongly correlated with high-temperature superconductivity. As mentioned in the structure analysis, the hydrogen in this $LaBeH_8$ could not be considered as a hydrogen-hydrogen connection framework, and thus the origin of the hydrogen-dominated DOS at (E_f) should be different from that previously found in clathrate hydrides. Meanwhile, this unusual molecular $[BeH_8]^{2-}$ unit is notably hydrogen rich and exhibits high symmetry which motivates us to conduct a molecular orbital (MO) analysis of $[BeH_8]^{2-}$ to gain a deeper understanding of its electronic properties (the detailed analysis is demonstrated in the Supplemental Material [59]). The results show that the molecular orbitals of the $[BeH_8]^{2-}$ unit directly contribute to eight electronic bands over an energy range between −14 eV and E_f. As shown in Figs. 2(c) and S4 [59], these bands originate from a low-lying singlet Be-H bonding state (A_{1g}), a singlet H-H bonding state between adjacent $[BeH_8]^{2-}$ anions (A_{2u}), a triplet Be-H bonding state (T_{1u}), and a partially occupied triplet state derived

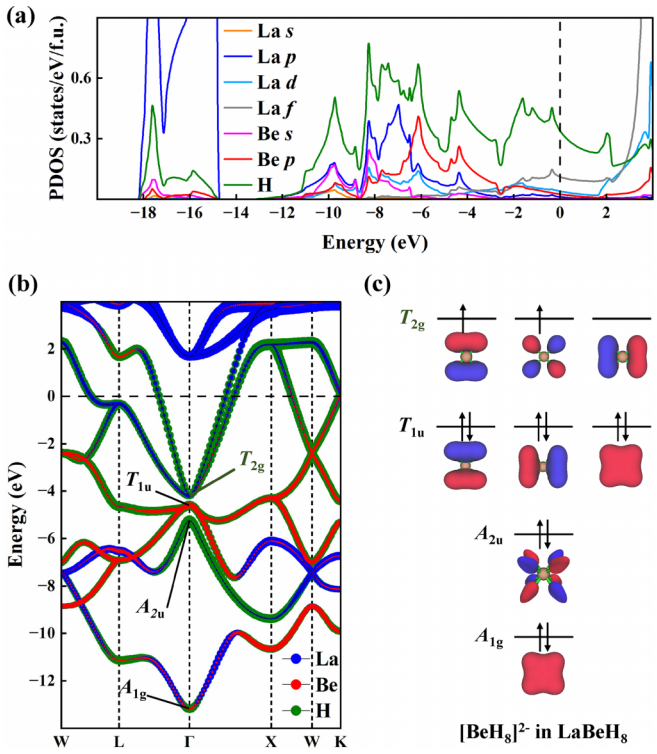

FIG. 2. (a) The orbital projected density of states (PDOS) of $LaBeH_8$ at 80 GPa. (b) Electronic energy band structure of $LaBeH_8$. (c) Molecular orbital (MO) diagram of the $[BeH_8]^{2-}$ hydride units in $LaBeH_8$. In (b), the radii of colored dots are proportional to the weights of the corresponding element. In (c), the orbitals with different angular momenta are marked with different colors. The H-H bonding state between adjacent $[BeH_8]^{2-}$ units is represented by the A_{2u} orbital of a single BeH_8 molecule (the detailed MO analysis is shown in Supplemental Material [59]).

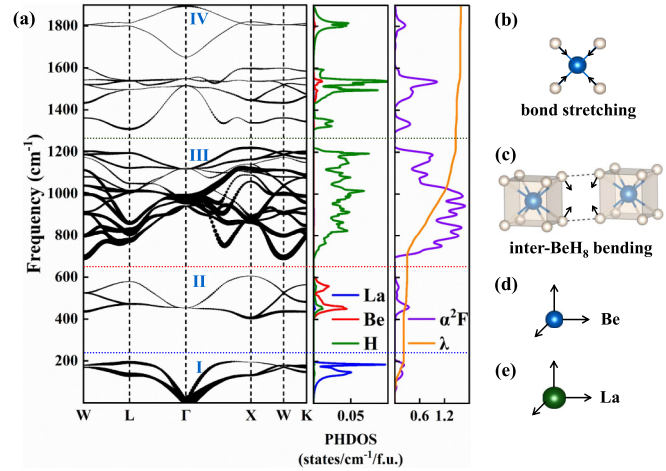

FIG. 3. (a) Phonon dispersion relations, element projected phonon density of states (PHDOS), and Eliashberg spectral function for $LaBeH_8$ at 80 GPa. The phonon states are divided into four sections by colored dashed lines. These sections result from (b) H vibrations along Be-H bonds and (c) perpendicular to Be-H bonds, (d) vibrations of Be ions, and (e) vibrations of La ions, contributing 8%, 74%, 5%, and 13% to the large EPC constant λ of 1.6, respectively. The calculated T_c (114 K at 80 GPa) agrees well with the previous simulations in Refs. [36,41].

only from H atoms (T_{2g}), respectively. There are only three bands to cross the E_f [Figs. 2(b) and S2] [59], which stem from the atomic hydrogen state (T_{2g}) in the $[BeH_8]^{2-}$ unit. It indicates that the partially filled $[BeH_8]^{2-}$ T_{2g} state leads to the intrinsic metallic feature in the solid, thereby resulting in a high hydrogen-dominated density of states at E_f. This unusual molecular $[BeH_8]^{2-}$ unit mimics the electronic behavior of atomic metallic hydrogen [42–46] and thus contributes to the high-temperature superconductivity in $LaBeH_8$.

To further unlock the origin of high-temperature superconductivity for $LaBeH_8$, we performed electron-phonon coupling (EPC) simulations, including phonon dispersion, projected phonon density of states (PHDOS), as well as the Eliashberg spectral function, at the experimentally synthesized pressures of 80–120 GPa [Figs. 3(a) and S3]. First, it is found that the estimated T_c decreases with increasing pressure, as shown in Table S3 [59], coinciding with previous results [36,41]. This validates the accuracy of our first-principles calculations. Hereafter, we have conducted a group-theoretical symmetry analysis on the phonon modes at 80 GPa [see Table I and Figs. 3(b)–3(e)]. We also provided the visualized

TABLE I. The symmetry assignment, corresponding theoretical vibrational band positions, and main atomic motions of the vibrational modes at the Γ point in $LaBeH_8$. The main atomic motions are identified from DFT calculations and symmetry group theory (Fig. S7) [59].

Symmetry	Frequency (cm^{-1})	Main atonic motions
T_{1u}	0	La (**r**)
T_{1u}	453	Be (**r**)
T_{1u}	941	H-Be-H scissorlike bending, H (**r**) in [111]
T_{2g}	962	H-Be-H rotation, BeH_8 squeezing in [111]
E_u	976	H-Be-H scissorlike bending, BeH_8 twisting in [100]
E_g	977	H-Be-H rotation, BeH_8 squeezing in [100]
T_{2u}	1117	H-Be-H scissorlike bending, BeH_8 twisting in [111]
T_{1g}	1121	H-Be-H rotation, BeH_8 rotation in [111]
T_{2g}	1515	Be-H stretching, BeH_8 squeezing in [111]
T_{1u}	1548	Be-H stretching, H (**r**) and Be (−**r**) in [111]
A_{1u}	1651	Be-H stretching, BeH_4 tetrahedra breathing
A_{1g}	1894	Be-H stretching, BeH_8 cube breathing

vibrational eigenvectors at the Γ point, as shown in Fig. S7 [59]. By vibrational frequencies, the phonon dispersion curves are basically split into regions I, II, III, and IV, as shown in Fig. 3(a) (the detailed analysis of each region is demonstrated in the Supplemental Material [59]). Of particular interest is region III with the vibrational frequencies ranging from 690 to 1220 cm^{-1}, owing to its notable contribution on the EPC constant as large as 74%. In such a region, the phonon modes predominantly result from the movements of H ions. For instance, the modes at the Γ point in region III [Figs. S7(c)–S7(h) [59]] are the vibrations of H ions perpendicular to Be-H bonds. Considering the collective motions of hydrogen ions in the crystal, these modes can be viewed as the inter-BeH_8 hydrogen-hydrogen vibrations, as shown in Fig. 3(c). As a consequence, such intermolecular vibrations between BeH_8 units are crucial for the strong electron-phonon coupling (EPC) in $LaBeH_8$.

Furthermore, we conducted additional simulations to estimate the frequency of H-H vibrations at various H-H distances in a one-dimensional hydrogen atomic chain. This analysis offers the relevant information supporting the hypothesis that vibrations in region III originate from the weak intermolecular H-H interactions between $[BeH_8]^{2-}$ units. As shown in Fig. S8 [59], the simulated frequencies are almost the same as the frequencies in this region (690–1220 cm^{-1}), which supports that the phonons in this unique frequency region are indeed dominated by weak H-H interactions between $[BeH_8]^{2-}$ units. All these results imply that the strong electron-phonon coupling in the system is attributed to the interactions between $[BeH_8]^{2-}$ units. In other words, the interactions between $[BeH_8]^{2-}$ units via weak H-H coupling play a critical role in the high-temperature superconductivity for $LaBeH_8$ at submegabar pressures.

In fact, we found that previously predicted $BaReH_9$ consists of hydrogen-rich $[ReH_9]^{2-}$ units similar to hydrogen-rich $[BeH_8]^{2-}$ units in $LaBeH_8$, while it possesses a rather low T_c compared with $LaBeH_8$ [26–28]. We further study their electronic properties to elucidate the origin of such a large-T_c difference for two hydrogen-rich salt structures. The $[ReH_9]^{2-}$ unit in $BaReH_9$ exhibits a fully filled 18-electron shell at ambient pressure [61,62], which is different from $LaBeH_8$ that shows the intrinsic metallic feature in the simulated electronic structure. With increasing pressure, insulated $BaReH_9$ was found to undergo a pressure-induced electronic band closure and exhibit a weak metallic phase, rendering a low hydrogen-derived density of states as shown in Fig. S9 [59] and thus a low T_c. These results suggest that the intrinsic metallic nature of saltlike ternary hydrides is a key to high-temperature superconductivity.

Finally, the stability of high-T_c $LaBeH_8$ at submegabar pressures is unexpected and its origin remains to be determined. The formation of $LaBeH_8$ could be viewed as the introduction of additional Be atoms into the H_8 cube of LaH_{10}, thereby forming covalent Be-H bonding. Moreover, we also found that H_{32} cages in LaH_{10} are not densely packed and thus the Be atoms could be inserted into the interstitial region of LaH_{10} as shown in Fig. 4(a), where the resultant close packing is also a key to the stability of the system at submegabar pressures. To verify this hypothesis, on the one hand, we have performed simulations on the enthalpy

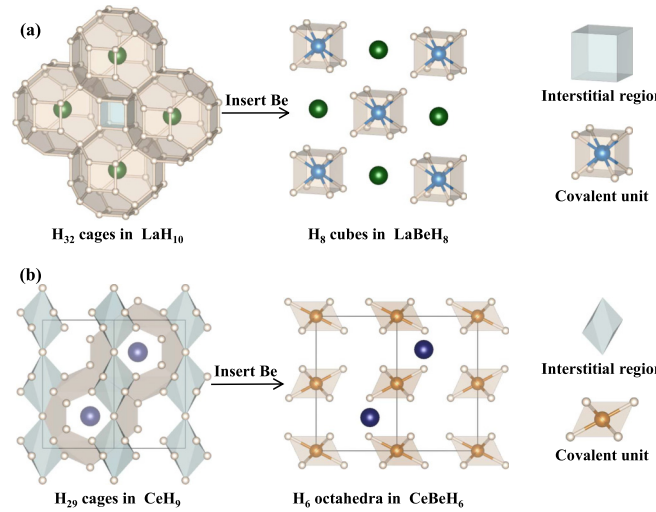

FIG. 4. Structural association between clathrate hydrides and ternary hydrides.

of LaH_{10}, $LaBeH_8$, CeH_9, and $CeBeH_6$. The results indicate these ternary hydrides are much more stable than the corresponding clathrate hydrides, as shown in Table S4 [59]. On the other hand, we further scrutinize a similar clathrate CeH_9 structure, where H_{29} is not densely packed as well. A similar operation by inserting Be atoms into the interstitial region of CeH_9 could result in a $P6_3/mmc$-$CeBeH_6$ structure as reported in Ref. [38]. In addition, there was a high-temperature superconducting phase $P\bar{3}m1$-$LaBH_7$ predicted in the La-B-H system [31], which adopts a similar structure to $CeBeH_6$. These results indicate the stability of $LaBeH_8$ might lie in the emergence of a covalent $[BeH_8]^{2-}$ unit.

IV. CONCLUSIONS

In conclusion, our comprehensive study reveals that $LaBeH_8$ could be viewed as a salt configuration of $La^{2+}[BeH_8]^{2-}$. Our molecular orbital analysis indicates a partially filled atomic hydrogen state (T_{2g}) in the molecular $[BeH_8]^{2-}$ unit results in the high hydrogen-dominated density of states at E_f, which mimics the electronic behavior of atomic metallic hydrogen. Our electron-phonon simulations reveal that the intermolecular H-H interactions between BeH_8 units play a critical role in the high-temperature superconductivity in $LaBeH_8$. Our further analysis suggests the unexpected stability of $LaBeH_8$ lies in the emergence of covalent BeH_8 units at submegabar pressures. The present results not only deepen our understanding of the origin of the unexpected stability and high-temperature superconductivity of $LaBeH_8$, but also offer guidance in the search for high-temperature superconductivity in a variety of ternary hydrides containing metallic covalent hydrogen-rich units at submegabar pressures.

ACKNOWLEDGMENTS

This research was supported by the National Natural Science Foundation of China (Grants No. 52288102, No. 52090024, No. 12074138, and No. 12374009), the Strategic

Priority Research Program of Chinese Academy of Sciences (Grant No. XDB33000000), the Fundamental Research Funds for the Central Universities, Program for Jilin University Science and Technology Innovative Research Team (2021TD-05), and computing facilities at the High-Performance Computing Centre of Jilin University.

[1] H. Wang, X. Li, G. Gao, Y. Li, and Y. Ma, WIREs Comput. Mol. Sci. **8**, e1330 (2018).
[2] D. Duan, Y. Liu, Y. Ma, Z. Shao, B. Liu, and T. Cui, Natl. Sci. Rev. **4**, 121 (2017).
[3] T. Ishikawa, T. Miyake, and K. Shimizu, Phys. Rev. B **100**, 174506 (2019).
[4] J. A. Flores-Livas, L. Boeri, A. Sanna, G. Profeta, R. Arita, and M. Eremets, Phys. Rep. **856**, 1 (2020).
[5] J. Lv, Y. Sun, H. Liu, and Y. Ma, Matter Radiat. Extremes **5**, 068101 (2020).
[6] X. Zhang, Y. Zhao, F. Li, and G. Yang, Matter Radiat. Extremes **6**, 068201 (2021).
[7] X. Zhong, J. S. Tse, R. J. Hemley, and H. Liu, The Innovation **3**, 100226 (2022).
[8] M. Du, W. Zhao, T. Cui, and D. Duan, J. Phys.: Condens. Matter **34**, 173001 (2022).
[9] K. P. Hilleke and E. Zurek, J. Appl. Phys. **131**, 070901 (2022).
[10] X. Zhang, Y. Zhao, and G. Yang, WIREs Comput. Mol. Sci. **12**, e1582 (2022).
[11] Y. Sun, X. Zhong, H. Liu, and Y. Ma, Natl. Sci. Rev. **11**, nwad270 (2024).
[12] Y. Wang, J. Lv, L. Zhu, and Y. Ma, Phys. Rev. B **82**, 094116 (2010).
[13] Y. Wang, J. Lv, L. Zhu, and Y. Ma, Comput. Phys. Commun. **183**, 2063 (2012).
[14] H. Wang, J. S. Tse, K. Tanaka, T. Iitaka, and Y. Ma, Proc. Natl. Acad. Sci. USA **109**, 6463 (2012).
[15] L. Ma, K. Wang, Y. Xie, X. Yang, Y. Wang, M. Zhou, H. Liu, X. Yu, Y. Zhao, H. Wang, G. Liu, and Y. Ma, Phys. Rev. Lett. **128**, 167001 (2022).
[16] Z. Li, X. He, C. Zhang, X. Wang, S. Zhang, Y. Jia, S. Feng, K. Lu, J. Zhao, J. Zhang, B. Min, Y. Long, R. Yu, L. Wang, M. Ye, Z. Zhang, V. Prakapenka, S. Chariton, P. A. Ginsberg, J. Bass *et al.*, Nat. Commun. **13**, 2863 (2022).
[17] F. Peng, Y. Sun, C. J. Pickard, R. J. Needs, Q. Wu, and Y. Ma, Phys. Rev. Lett. **119**, 107001 (2017).
[18] Y. Li, J. Hao, H. Liu, J. S. Tse, Y. Wang, and Y. Ma, Sci. Rep. **5**, 9948 (2015).
[19] P. Kong, V. S. Minkov, M. A. Kuzovnikov, A. P. Drozdov, S. P. Besedin, S. Mozaffari, L. Balicas, F. F. Balakirev, V. B. Prakapenka, S. Chariton, D. A. Knyazev, E. Greenberg, and M. I. Eremets, Nat. Commun. **12**, 5075 (2021).
[20] I. A. Troyan, D. V. Semenok, A. G. Kvashnin, A. V. Sadakov, O. A. Sobolevskiy, V. M. Pudalov, A. G. Ivanova, V. B. Prakapenka, E. Greenberg, A. G. Gavriliuk, I. S. Lyubutin, V. V. Struzhkin, A. Bergara, I. Errea, R. Bianco, M. Calandra, F. Mauri, L. Monacelli, R. Akashi, and A. R. Oganov, Adv. Mater. **33**, 2006832 (2021).
[21] Y. Wang, K. Wang, Y. Sun, L. Ma, Y. Wang, B. Zou, G. Liu, M. Zhou, and H. Wang, Chin. Phys. B **31**, 106201 (2022).
[22] E. Snider, N. Dasenbrock-Gammon, R. McBride, X. Wang, N. Meyers, K. V. Lawler, E. Zurek, A. Salamat, and R. P. Dias, Phys. Rev. Lett. **126**, 117003 (2021).
[23] H. Liu, I. I. Naumov, R. Hoffmann, N. Ashcroft, and R. J. Hemley, Proc. Natl. Acad. Sci. USA **114**, 6990 (2017).
[24] A. Drozdov, P. P. Kong, V. S. Minkov, S. P. Besedin, M. A. Kuzovnikov, S. Mozaffari, L. Balicas, F. F. Balakirev, D. E. Graf, V. B. Prakapenka, E. Greenberg, D. A. Knyazev, T. Tkacz, and M. I. Eremets, Nature (London) **569**, 528 (2019).
[25] M. Somayazulu, M. Ahart, A. K. Mishra, Z. M. Geballe, M. Baldini, Y. Meng, V. V. Struzhkin, and R. J. Hemley, Phys. Rev. Lett. **122**, 027001 (2019).
[26] G. Markopoulos, P. Kroll, and R. Hoffmann, J. Am. Chem. Soc. **132**, 748 (2010).
[27] T. Muramatsu, W. K. Wanene, M. Somayazulu, E. Vinitsky, D. Chandra, T. A. Strobel, V. V. Struzhkin, and R. J. Hemley, J. Phys. Chem. C **119**, 18007 (2015).
[28] E. A. Vinitsky, T. Muramatsu, M. Somayazulu, W. K. Wanene, Z. Liu, D. Chandra, and R. J. Hemley, J. Phys.: Condens. Matter **28**, 505701 (2016).
[29] D. Meng, M. Sakata, K. Shimizu, Y. Iijima, H. Saitoh, T. Sato, S. Takagi, and S.-i. Orimo, Phys. Rev. B **99**, 024508 (2019).
[30] S. Di Cataldo, C. Heil, W. von der Linden, and L. Boeri, Phys. Rev. B **104**, L020511 (2021).
[31] X. Liang, A. Bergara, X. Wei, X. Song, L. Wang, R. Sun, H. Liu, R. J. Hemley, L. Wang, G. Gao, and Y. Tian, Phys. Rev. B **104**, 134501 (2021).
[32] M. Gao, X.-W. Yan, Z.-Y. Lu, and T. Xiang, Phys. Rev. B **104**, L100504 (2021).
[33] S. Di Cataldo, W. von der Linden, and L. Boeri, npj Comput. Mater. **8**, 2 (2022).
[34] Y. Sun, Y. Wang, X. Zhong, Y. Xie, and H. Liu, Phys. Rev. B **106**, 024519 (2022).
[35] S. Li, H. Wang, W. Sun, C. Lu, and F. Peng, Phys. Rev. B **105**, 224107 (2022).
[36] Z. Zhang, T. Cui, M. J. Hutcheon, A. M. Shipley, H. Song, M. Du, V. Z. Kresin, D. Duan, C. J. Pickard, and Y. Yao, Phys. Rev. Lett. **128**, 047001 (2022).
[37] R. Lucrezi, S. Di Cataldo, W. von der Linden, L. Boeri, and C. Heil, npj Comput. Mater. **8**, 119 (2022).
[38] Q. Jiang, Z. Zhang, H. Song, Y. Ma, Y. Sun, M. Miao, T. Cui, and D. Duan, Fundamental Research **4**, 550 (2024).
[39] L. Liu, F. Peng, P. Song, X. Liu, L. Zhang, X. Huang, C. Niu, C. Liu, W. Zhang, Y. Jia, and Z. Zhang, Phys. Rev. B **107**, L020504 (2023).
[40] T. Ma, Z. Zhang, M. Du, Z. Huo, W. Chen, F. Tian, D. Duan, and T. Cui, Mater. Today Phys. **38**, 101233 (2023).
[41] Y. Song, J. Bi, Y. Nakamoto, K. Shimizu, H. Liu, B. Zou, G. Liu, H. Wang, and Y. Ma, Phys. Rev. Lett. **130**, 266001 (2023).
[42] C. J. Pickard and R. J. Needs, Nat. Phys. **3**, 473 (2007).
[43] L. Zhang, Y. Niu, Q. Li, T. Cui, Y. Wang, Y. Ma, Z. He, and G. Zou, Solid State Commun. **141**, 610 (2007).
[44] J. M. McMahon and D. M. Ceperley, Phys. Rev. Lett. **106**, 165302 (2011).

[45] J. M. McMahon and D. M. Ceperley, Phys. Rev. B **84**, 144515 (2011).
[46] H. Liu, H. Wang, and Y. Ma, J. Phys. Chem. C **116**, 9221 (2012).
[47] G. Kresse and J. Furthmüller, Phys. Rev. B **54**, 11169 (1996).
[48] J. P. Perdew and Y. Wang, Phys. Rev. B **45**, 13244 (1992).
[49] J. P. Perdew, K. Burke, and M. Ernzerhof, Phys. Rev. Lett. **77**, 3865 (1996).
[50] V. L. Deringer, A. L. Tchougréeff, and R. Dronskowski, J. Phys. Chem. A **115**, 5461 (2011).
[51] V. Wang, N. Xu, J. C. Liu, G. Tang, and W. T. Geng, Comput. Phys. Commun. **267**, 108033 (2021).
[52] S. Baroni, S. de Gironcoli, A. Dal Corso, and P. Giannozzi, Rev. Mod. Phys. **73**, 515 (2001).
[53] P. Giannozzi, S. Baroni, and N. Bonini, J. Phys.: Condens. Matter **21**, 395502 (2009).
[54] G. Kresse and D. Joubert, Phys. Rev. B **59**, 1758 (1999).
[55] P. B. Allen and R. C. Dynes, Phys. Rev. B **12**, 905 (1975).
[56] G. M. Éliashberg, Sov. Phys. JETP **11**, 696 (1960).
[57] A. D. Becke and K. E. Edgecombe, J. Chem. Phys. **92**, 5397 (1990).
[58] K. Parlinski, Z. Q. Li, and Y. Kawazoe, Phys. Rev. Lett. **78**, 4063 (1997).
[59] See Supplemental Material at http://link.aps.org/supplemental/10.1103/PhysRevB.109.214506 for a detailed analysis of the chemical bonding, molecular orbitals, phonon dispersion, and electron-phonon coupling.
[60] L. Liu, C. Wang, S. Yi, K. W. Kim, J. Kim, and J.-H. Cho, Phys. Rev. B **99**, 140501(R) (2019).
[61] W. Bronger, Angew. Chem., Int. Ed. Engl. **30**, 759 (1991).
[62] K. Yvon, Chimia **52**, 613 (1998).